© 2011

STRUCTURE-SENSITIVE MECHANISM
OF NANOGRAPHENE FAILURE

E. F. Sheka [a,*], **N. A. Popova** [a], **V. A. Popova** [a], **E. A. Nikitina** [a,b], **L. H. Shaymardanova** [a]

[a] *Peoples' Friendship University of Russia*
117198, Moscow, Russia

[b] *Institute of Applied Mechanics, Russian Academy of Sciences*
119991, Moscow, Russia

The quantum-mechanochemical-reaction-coordinate approach has disclosed atomically matched peculiarities that accompany the deformation–failure–rupture process occurring in nanographenes. The high stiffness of the graphene body is provided by the benzenoid unit. The anisotropy of the unit mechanical behavior in combination with different configurations of the unit packing with respect to the body C–C bond chains forms the ground for the structure-sensitive mechanism of the mechanical behavior that is drastically different for two different deformation modes. The zig-zag deformation mode is particularly manifested with the formation of one-atom chains. The approach allows tracing a deformation-stimulated change in the chemical reactivity of both the nanographene body and its individual atoms.

1. INTRODUCTION

In contrast to real physical experiments, when changing the object shape under loading is monitored, computational experiments usually deal with the total energy response to the object shape deformation that simulates either tension and contraction or bending, screwing, shift, and so on. As regards graphene and carbon nanotubes (CNTs), whose mechanical properties are amenable to experimental study with difficulty, the computational experiments takes on great significance.

Numerous works devoted to the calculation of mechanical properties of nanographenes and CNTs underlie two approaches, the continuum and atomistic ones. The continuum approach is based on the well-developed theory of elasticity of continuous solid media applied to shells, plates, beams, rods, and trusses. These are structure elements used for the continuum description. Nanoscale continuum methods (see Refs. [1–5] and the references therein), among which those based on the structural mechanics concept [6] are the most developed, have shown the best ability to simulate nanostructure materials. In accordance with this concept, CNT and graphene are geometrical framelike struc-

tures where the primary bonds between two nearest-neighbor atoms act like load-bearing beam members, whereas an individual atom acts as the joint of the related beams [7–10].

The basic concept of the atomistic approach consists in obtaining mechanical parameters of the object from results of the direct solutions of either the Newton motion laws [10, 11] or the Schrödinger equations [12–14] under changing the object shape following a particular algorithm that simulates a the desired deformation type. Mechanical properties are revealed from the strain energy

$$E_s(\varepsilon) = E_{tot}(\varepsilon) - E_{tot}(0), \qquad (1)$$

where $E_{tot}(0)$ and $E_{tot}(\varepsilon)$ are the total energies of the unloaded sample and of the sample subjected to ε strain. The stretching algorithms are subordinated to the manner of the object structure presentation. For example, the main platform of the density functional theory (DFT) calculations consists in treating all structures having a supercell geometry using the periodic boundary conditions. The sample stretching is achieved by increasing the optimized lattice constant c of the supercell in a regular manner and by uniformly expanding the atomic structure obtained from previous optimization. Not the energy itself, but forces applied

to atoms become the main goal of calculations. Within the DFT technique, the tension force is determined as

$$F_T = -\frac{\partial E_s(\varepsilon)}{\partial c}. \tag{2}$$

These forces are subsequently input into the relations of macroscopic linear theory of elasticity and lay the foundation for the evaluation of micro-macroscopic mechanical parameters such as the Young modulus E, the Poisson ratio ν, and so on. We note that the parameters E and ν obviously differ from those determined within the continuous approach, and their coincidence is purely accidental. The modern translation-boundary-condition DFT approach is solid-state by nature, which is particularly clear from its extension to the case of phonon instability of the graphene body [2], particularly in the manner of phonon mode softening [15]. This offers an additional dynamic view on the graphene failure mechanism from the standpoint of phase transitions.

In this paper, we suggest to go beyond the solid-state approach as well as beyond the conventional energy-strain-response concept and to consider the mechanism of the tensile deformation leading to the failure and rupture of a nanographene body in the course of a mechanochemical reaction occurring with this macromolecule. A similarity between mechanically induced reactions and the first-type chemical ones, first pointed out by Tobolski and Eyring more than sixty years ago [16], suggests the use of a well-developed quantum-chemical approach of the reaction coordinate [17] in the study of the atomic structure transformation under deformation. First applied to the deformation of poly(dimethylsiloxan) oligomers [18], the approach has revealed a high efficacy in disclosing the mechanism of failure and rupture of the considered polymers.

2. MECHANOCHEMICAL INTERNAL COORDINATES

The main point of the approach is in the definition of the reaction coordinate. In chemical reactions, that coordinate is usually selected among the internal ones (valence bond, bond angle, or torsion angle) or is presented as a linear combination of them. Similarly, mechanochemical internal coordinates (MICs) were introduced as modified internal coordinates defined so as to allow specifying the considered deformational modes [18, 19]. The MICs thus designed have to meet the following requirements.

1. Every MIC is a classifying mark of a deformational mode: uniaxial tension and contraction are de-

scribed by linear MICs similar to valence bonds, bending is characterised by a MIC similar to the valence angle, and screwing is attributed to MICs similar to torsion angles.

2. Every MIC is determined in much the same way as the other internal coordinates except a set of specially selected support atoms.

3. The MIC relevant to a particular deformational mode is excluded from the quantum-chemical optimization procedure in seeking the minimum of the total energy.

4. A response force is determined as the residual gradient of the total energy along the selected MIC. This logic is dictated by the general architecture of the conventional quantum-chemical software, where the force calculation (more specifically, the total energy gradient calculation) is the key procedure.

Implementation of the MIC concept in the framework of DYQUAMECH software [20], which is based on the Hartree–Fock (HF) unrestricted version of the CLUSTER-Z1 codes exploiting advanced semiempirical quantum-chemical methods [21], provides (i) an MIC input algorithm, (ii) computation of the total energy gradients in both the Cartesian and internal coordinates, and (iii) an optimization performance in the internal coordinates. Additionally, the program retains all features of the unrestricted broken symmetry (UBS) approach, particularly important for odd electronic systems of CNTs [22] and graphene [23]. We note that all DFT calculations, except the recent one in [14], were performed in the framework of restricted versions of the programs that do not take the graphene odd-electron spins into account and hence ignore the correlation interaction between these electrons. The peculiarities of the graphene odd-electron behavior are related with a considerable extension of its C–C distances, which in turn causes a noticeable weakening of the odd-electron interaction and thus requires taking the correlation interaction between these electrons into account [23].

3. CALCULATION OF THE RESPONSE FORCE

The forces, which are the first derivatives of the electron energy $E(R)$ with respect to the Cartesian coordinates R of an atom, are determined as [20]

$$\frac{dE}{dR} = \langle\phi|\frac{\partial H}{\partial R}|\phi\rangle + 2\langle\frac{\partial\phi}{\partial R}|H|\phi\rangle + 2\langle\frac{\partial\phi}{\partial P}|H|\phi\rangle\frac{dP}{dR}, \tag{3}$$

where ϕ is the electron wave function of the ground state, H represents the adiabatic electron Hamiltonian, and P is the nucleus momentum. Derivatives are determined for fixed atomic positions. In calculating

(3), a quite efficient computational technique suggested in [24] was used. The DYQUAMECH algorithm of the force determination concerns forces applied to each ith MIC. These partial forces F_i are used afterwards for determining all the sought micro-macroscopic mechanical characteristics related to uniaxial tension, i. e., response force F,

$$F = \sum_i F_i, \qquad (4)$$

stress σ,

$$\sigma = \frac{F}{S} = \frac{1}{S} \sum_i F_i, \qquad (5)$$

where S is the loading area; the Young modulus E^*,

$$E^* = \sigma / \varepsilon, \qquad (6)$$

where $\varepsilon = \Delta L_i / L_0$ is the strain, L_0 is the initial MIC length and ΔL_i is the elongation of the ith MIC and is identical to all MICs in the current experiment; stiffness coefficient k,

$$k = F / \Delta L_i. \qquad (7)$$

A completed computational cycle provides the following data.

Microscopic characteristics that include (i) the atomic structure of the loaded graphene body at any stage of the deformation including bond scission and post-breaking relaxation; (ii) the strain energy E_s, Eq. (1), and both total (4) and partial response forces; (iii) molecular and atomic chemical susceptibilities of the body expressed in terms of the total N_D and atomically partitioned N_{DA} numbers of effectively unpaired electrons [25]. Because both the UBS HF in the current study and the spin-polarized DFT in [14] belong to single-determinant techniques [22, 25], the appearance of a nonzero number of effectively unpaired electrons is just another face of the spin density ρ determined in [14]. Both values are just a manifestation of the spin-mixed character of the singlet UBS solutions. It is unrelated to the magnetic properties of the object [23] stated in [14], but can be self-consistently used to describe the reactivity of the object atoms. The energy, force, N_D, and(or) N_{DA} versus elongation dependences exhibit mechanical behavior of the object at all stages of the deformation considered at the atomic level. The last two dependences represent changes in the chemical activity of the body and its atoms in the course of deformation.

Micro-macroscopic characteristics involve stress–strain interrelations in terms of Eqs. (5)–(7) that allow introducing convenient mechanical parameters similar to those of the elasticity theory.

4. GRAPHENE AS A SUBJECT OF MECHANICAL DEFORMATION

From the mechanics standpoint, the benzenoid hexagon structure of graphene raises two questions concerning (i) mechanical properties of the benzenoid unit in and of itself and its mechanical isotropy in particular, and (ii) the influence of the unit packing on the mechanical properties of graphene as a whole. Conventionally, the mechanical properties of benzenoid units are assumed to be completely isotropic due to the high symmetry of the unit structure [1–4]. But as shown recently [23], the unit exact symmetry in real nanographenes is much lower than D_{6h}, and hence the suggestion of its mechanical isotropy is rather questionable. Moreover, the conclusion about mechanical isotropy does not follow from the structural symmetry of the object because the object rupture is related with the scission of particular chemical bonds whose choice is dependent on the applied stress direction. To check the prediction, we consider the tensile deformation of the benzene molecule subjected to two uniaxial tension modes, referred to as zig-zag (zg, along the C–C bond) and arm chair (ach, normal to the C–C bond). These names have obviously been chosen in anticipation of zg and ach edges of a rectangular graphene sheet or ribbon. These and further calculations were performed by using the PM3 version of the DYQUAMECH program.

5. TENSILE DEFORMATION AND FAILURE OF THE BENZENE MOLECULE

Configurations of two MICs related to the ach and zg deformation modes are shown in Fig. 1. The deformation proceeds as a stepwise elongation of the MICs with the increment $\delta L = 0.05$ Å at each step, such that the current MIC length is $L = L_0 + n\delta L$, where n is the number of the deformation steps. One end of each MIC is fixed (on atoms 1 and 2 or 1 and 5 in the case of ach or zg modes, respectively). Consequently, these
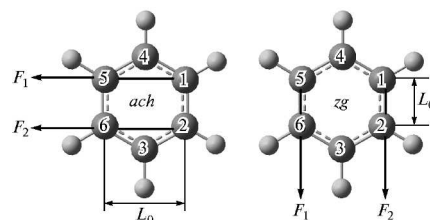

Fig. 1. Two MICs of an uniaxial tension of the benzene molecule for the ach and zg deformational modes. The two values of L_0 nominate the initial lengths of the MICs while F_1 and F_2 number the response forces
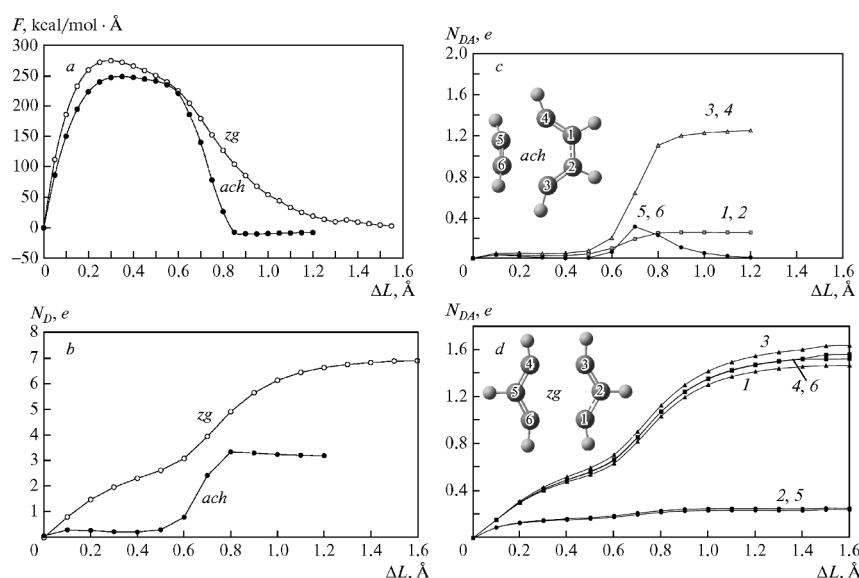
Fig. 2. Microscopic characteristics of the benzene molecule deformation. Figures near the curves in panels c and d correspond to the atom numbers on the inserted structures

atoms are immobilized, while atoms 5 and 6, and 2 and 6 move along the arrows and thus provide the MIC successive elongation, but do not participate in the optimization procedure at each elongation step. Figure 2 presents the two modes of elongation response of the total response force F in terms of Eq. (4) (Fig. 2a) and the total N_D (Fig. 2b) and partial N_{DA} numbers of unpaired electrons (Figs. 2c and 2d).

As can be seen in Fig. 2, the mechanical behavior of the molecule is highly anisotropic. The force-elongation dependence shown in Fig. 2a differs both in the initial linear region and at the final steps, exhibiting a considerable extension of the failure zone in the case of the zg mode in comparison with the ach one. Linear elastic behavior is highly restricted and is limited to the first one or two deformation steps. Even more radical difference is illustrated in Figs. 2b–2d, indicating a difference in the electronic processes that accompany the molecule failure. Obviously, these features are related with the difference in the MIC atomic compositions related to the two modes, which results in the difference in the structure of the molecular fragments formed under rupture. For the zg mode, two MICs are aligned along the C_1–C_6 and C_3–C_4 molecular bonds, and two atomically identical three-atom fragments are formed under rupture. For the zg mode, the MIC elongation is immediately transformed into the bond elongation. The C–C bond length 1.395 Å of the unstrained benzene molecule is just a bordering value, exceeding which violates the complete covalent coupling of the molecule odd electrons of two neighbor carbon atoms and causes

the appearance of effectively unpaired electrons [25]. That is why the increment value 0.05 Å is significant enough for the appearance of unpaired electrons even at the first step of elongation. The bond breaking occurs when the elongation reaches 0.2–0.3 Å (these values determine the maximum position of the force-elongation dependence in Fig. 2a), but the two three-atom radicals are stabilized only when the elongation exceeds 1.2 Å (see Fig. 2d).

In the case of the ach mode, the corresponding MICs connect atoms 1 and 5, and 2 and 6, and hence only about 40 % of the MIC elongation is transformed into that of each of the two C–C bonds that rest on the MIC. This explains why N_{DA} values on all carbon atoms are quite small in this case (Fig. 2c) until the MIC elongation ΔL suffices for bond breaking. Actually, the bond breaking is not an instant process and, as is seen in Fig. 2a, it starts at $\Delta L = 0.3$ Å and ends at $\Delta L = 0.6$ Å. Two-atom and four-atom fragments are formed when the molecule is broken. At the rupture moment, the two-atom fragment is a stretched acetylene molecule, which is assompanied by the presence of unpaired electrons on atoms 5 and 6 (see Fig. 2c) because the C–C bond length exceeds a critical value above which the covalent coupling of odd electrons is incomplete. However, further relaxation of the molecule structure at larger elongation shortens the bond, placing it below the critical value, and the unpaired electrons disappear. The second fragment is a biradical whose structure is stabilized at $\Delta L = 0.9$ Å.

Therefore, the zg and ach modes of the tensile de-

Table. Micro-macroscopic mechanical characteristics of benzene molecule and (5,5) nanographene[1)]

	Critical elongation, nm	Critical force of response F_{cr}, 10^{-9} N	Stress σ, 10^9 N/m^2	Stiffness coefficient k,N/m	Young's modulus E^*,TPa
Benzene zg mode	0.27	12.54	153.72	46.46	3.2
Benzene ach mode	0.38	9.82	206.31	25.84	4.23
(5,5) graphene zg mode	1.47	45.08	116.18	30.66	1.14
(5,5) graphene ach mode	1.50	50.09	129.11	33.40	1.20
H-terminated (5,5) graphene zg mode	1.38	47.29	121.89	34.27	1.33
H-terminated (5,5) graphene ach mode	1.56	54.53	140.53	34.95	1.24

[1)] The critical elongation corresponds to the position of the first zero values of the response force first derivative over the elongation. Stress and stiffness coefficients are determined at the critical response force. The Young moduli are determined as slope-angle tangents of the stress–strain curves at the first steps of deformation.

formation of the benzene molecule occur as absolutely different mechanochemical reactions. Besides the difference in the microscopic behavior, the two modes are characterized by different mechanical parameters in terms of Eqs. (4)–(7), whose values are given in Table. Taken together, the obtained results are evidence of a sharp mechanical anisotropy of the benzene molecule in the direction of the load application and of an extremely high stiffness of the molecule. Actually, the considered deformational modes of the benzene molecule do not exactly reproduce similar situations for benzenoid units in CNTs and graphene, but the zg and ach edge-structure dependence of the mechanical behavior of both CNTs [2, 26, 27] and graphene [4, 28, 29] is largely determined by the mechanical anisotropy of the benzene molecule.

6. TENSILE DEFORMATION OF NANOGRAPHENE

The benzenoid pattern of graphene sheets and the regular packing of units predetermine the choice of either parallel or normal MIC orientation to the chain of C–C bonds, similarly to those introduced in studying the benzene molecule. In the rectangular nanographene sheets and nanoribbons, the parallel orientation corresponds to tensile deformation applied to the zg edges, while the normal one should be attributed to the ach edges. The MIC configurations of the ach and zg tensile modes of the (5,5) nanographene sheet are presented in Fig. 3. The computational procedure was fully identical to the one described above for the benzene molecule, with the only difference in the step in-
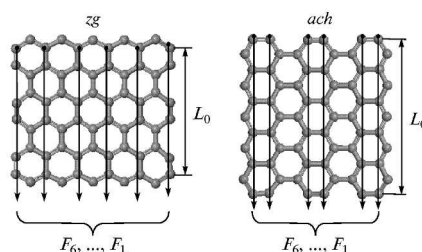

Fig. 3. Six MICs of uniaxial tension of the (5,5) nanographene for the ach and zg deformational modes
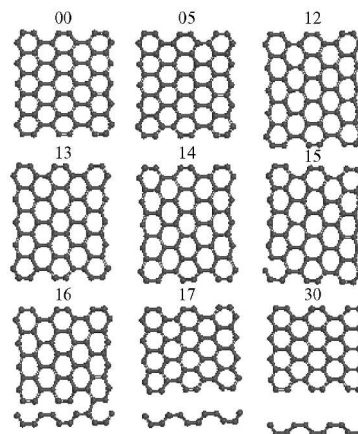

Fig. 4. Structures of the $(5, 5)$ nanographene under the successive steps of the ach deformation regime. Figures mark the step numbers

crement $\delta L = 0.1$ Å. The loading area is determined as $S = D L_0^{z(a)}$, where $D = 3.35$ Å is the Van der Waals diameter of the carbon atom and $L_0^{z(a)}$ is the initial length of the MICs in the case of zg (ach) modes.
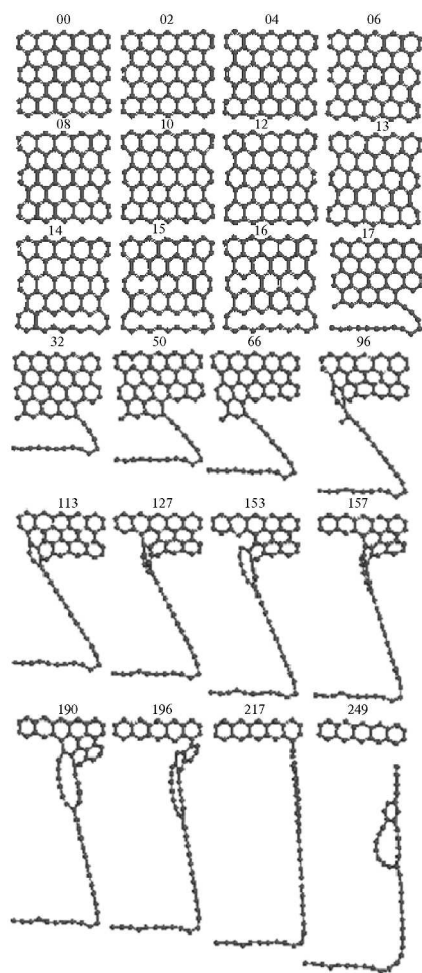
Fig. 5. The same as in Fig. 4 for the *zg* deformation regime

6.1. The *ach* mode of graphene tensile deformation

Figure 4 presents structure images of the selected set of deformation steps. The sheet is uniformly stretched in the course of the first 14 steps, and the first C–C bond breaking occurs at the 15th step. The breaking is completed at the 17th step and the final structure transformation looks like that occurring at a similar deformational mode of benzene: the sheet is divided into two fragments, one of which is a shortened (5,4) equilibrated nanographene and the other is a polymerized chain of acetylene molecules transferred into the carbine C=C bond chain.

6.2. The *zg* mode of graphene tensile deformation

Figure 5 presents the structure image of the selected set of successive deformation steps revealing an exciting picture of a peculiar failure of the graphene body with so drastic a difference in details compared to the *ach* mode that only a simplified analogy can assist in a concise description of the picture. The failure of tricotage seems to be a proper model. Actually, as known, the toughness of a tricotage sheet and the manner of its failure depend on the direction of the applied stress and the space configuration of its stitch packing. In this language, each benzenoid unit presents a stitch, and in the case of the *ach* mode, the sheet rupture is both commenced and completed by the rupture of a single stitch row. In the case of the *zg* mode, the rupture of one stitch is "tugging at thread" the other stitches that are replaced by a still elongated one-atom chain of carbon atoms. Obviously, this difference in the mechanical behavior is related to different configurations of the benzenoid packing with respect to the body C–C bond chains.

6.3. A comparative study of the *ach* and *zg* modes of the graphene tensile deformation

The difference in the structural pattern of the two deformation modes naturally leads to the difference in quantitative characteristics of the mechanical behavior in these two cases. Figure 6 shows the strain energy E_s, the total response force F, and the total number N_D of effectively unpaired electrons for both deformation modes as functions of the elongation ΔL. In contrast to the benzene molecule with no unpaired electrons in the unstrained ground state, the N_D value of unstrained nanographene is quite large [23]. Figure 6*c* shows the additional effect of the C–C bond elongation caused by the tensile deformation and manifests an increase in the chemical activity of the body in the course of deformation.

The first difference that follows from the analysis of the data in Fig. 6 is a drastic shortening of the deformation area under the *ach* deformation mode with respect the *zg* one (the difference in the ΔL scales in Fig. 6 for both modes). Obviously, this feature carries the peculiarity of the *zg* and *ach* mode behavior of the benzene molecule. While the *ach* deformation is one-stage and is terminated at the 20th step, the *zg* deformation is multi-stage and proceeds up to the 250th step followed by the saw-tooth shape of all three elongation dependencies, which reflects a successive stitch dissolution. This last is clearly seen in Fig. 5 that presents structures related to the steps corresponding to the force-elongation teeth maxima. The stitch dissolution is accompanied by a successive one-atom chain formation
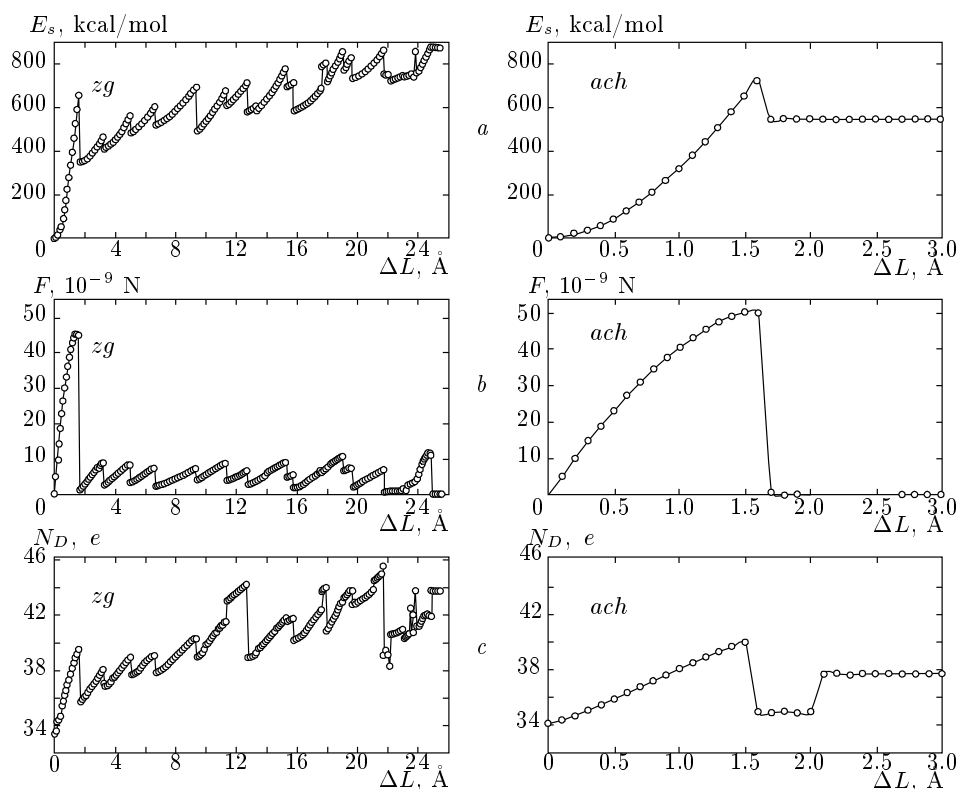
Fig. 6. Microscopic characteristics of the (5,5) nanographene deformation at zg (left) and ach (right) deformation modes: (a) strain energy according to Eq. (1); (b) response force as in Eq. (4); (c) the total number N_D of effectively unpaired electrons (see [22] for determination)

whose cracking at the 249th step completes the body rupture.

The formation of a one-atom chain under the deformation of a graphene nanoribbon was first observed in molecular dynamics calculations [11]. The deformation was performed similarly to the considered zg deformation mode. The deformation areas covered only a small part of a long ribbon. The next observation of one-atom chains occurred in UBS DFT calculations and concerned a big supercell equivalent to (4,10) nanographene [14]. As previously, the zg deformation mode was studied. Two one-atom fragments implanted in the deformed cell body were obtained in this case. These data taken together with those presented in Fig. 5 suggest that one-atom chains can be the main structural pattern of the zg regime of the graphene body deformation. Actually, this tendency was recently recorded experimentally [30, 31]. As can be seen from the figures presented in these papers and, in particular, in the movie that accompanies paper [31], experimentally observed formation of one-atom carbon chain occurs in the manner of the zg regime of the deformation.

The N_D dependences shown in Fig. 6c are clear evidence of the difference in the mechanochemical reactions related to the ach and zg deformation modes. The achieved saturation in the N_D values by the 21st step clearly witnesses the termination of the reaction in the ach case. In contrast, the zg reaction proceeds further with a saw-tooth-like N_D dependence that is highly similar to the dependence of both the strain energy and response force in Figs. 6a and 6b. Importantly, the discussed N_D dependences reflect a quantitative change in the chemical reactivity of the graphene body under tensile deformation.

7. TENSILE DEFORMATION OF HYDROGEN-TERMINATED (5,5) NANOGRAPHENE

Termination of the nanographene sheet edges by hydrogen atoms, preserving a qualitative picture of the nanographene mechanical behavior in general, is drastically different in the details. Figures 7 and 8 present structure images of the selected sets of defor-
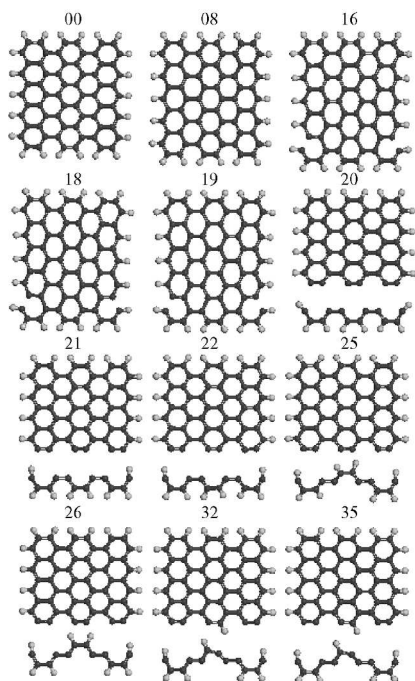
Fig. 7. Structures of the $(5, 5)$ H-terminated nanographene under successive steps of the *ach* deformation regime. Figures mark the step numbers
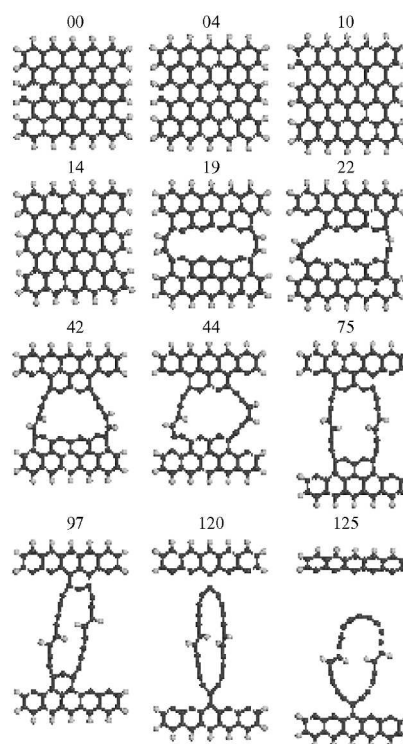

Fig. 8. The same as in Fig. 7 for the *zg* deformation regime

mation steps related to the *ach* and *zg* deformation of the H-terminated body. As can be seen in Fig. 7, the *ach* deformation mode proceeds similarly to the case of nonterminated graphene and is accomplished at the 20th step. The difference in the structure of the final fragments in Figs. 4 and 7 is evidently caused by the presence of hydrogen atoms in the latter case. Structures corresponding to steps from 26 to 35 obviously highlight a competition between the optimum hydrogen saturation of the split carbine chain and a strong tendency of the nanographene remainder to be hydrogenterminated. In contrast to this, the *zg* mode occurs quite differently in nonterminated graphene, while the one-atom chain pattern is clearly preserved. As can be seen in Fig. 8, the first broken C–C bond is located just in the center of the body. Further bond scission, as previously, leads to the formation of a one-atom chain of carbon atoms of a closed shape, whose splitting as a whole (see Fig. 8) from the body edge manifests the termination of the sheet failure. Although this action occurred at the 122th step, at a much greater elongation than for the *ach* mode, the elongation is twice less than that of nonterminated graphene. Therefore, the presence of hydrogen terminators shortens the deformation area quite significantly.

Figure 9 presents elongation-dependent response forces related to the *ach* and *zg* deformation modes. The observed dependences have much in common with those shown in Fig. 6 for nonterminated graphene. As can be seen in Fig. 9, the *ach* deformation mode occurs at one stage similarly to the case of nonterminated graphene. The *zg* deformation mode is multistage as previously, and all three elongation dependences have a characteristic saw-tooth shape. This shape character is evidently related to the formation of one-atom chains in both cases. Therefore, the *zg* deformation mode preserves its one-chain character for both empty-edge and H-terminated graphene bodies. At the same time, the presence of hydrogen atoms crucially affects the chain shape, thus changing the place of the first C–C bond scission. This causes the transformation of a long linear chain into a closed one.

The Table collects the main parameters related to the first stage of deformation of all studied samples. As can be seen from the table, at this stage, there is an obvious similarity in the behavior of both nonterminated and H-terminated sheets under both deformation modes. In support of this conclusion, Fig. 10 presents a comparative view on the microscopic characteristics related to the two deformation modes of a nontermi-
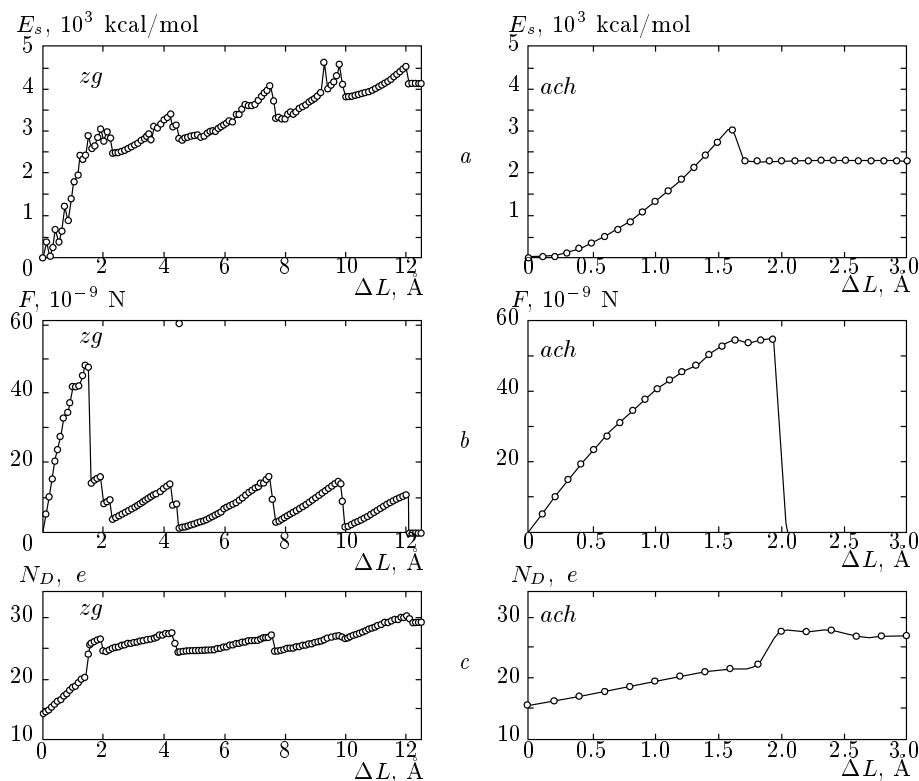
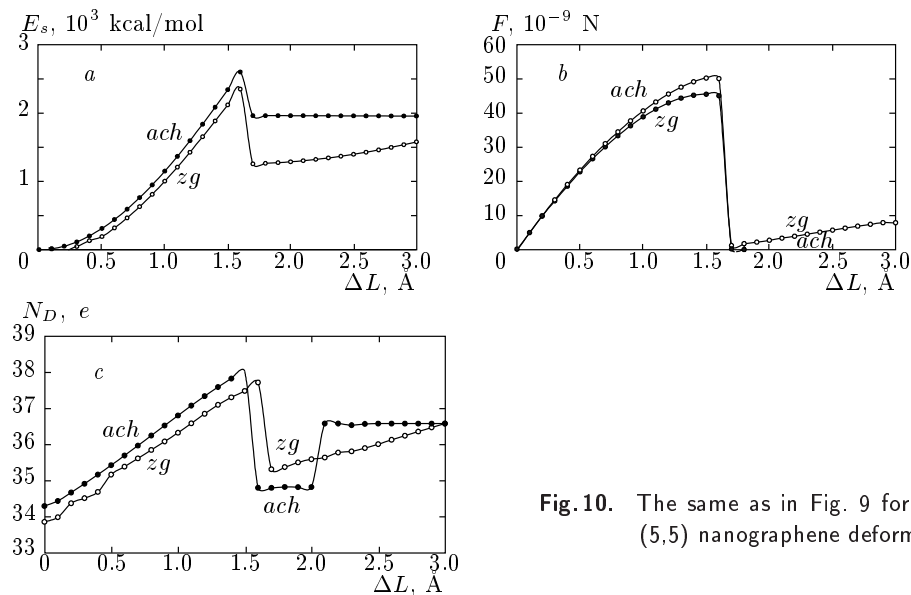**Fig. 9.** The same as in Fig. 6 for the (5,5) H-terminated nanographene

Fig. 10. The same as in Fig. 9 for the first stage of (5,5) nanographene deformation

nated sample. An obvious similarity in the characteristic behavior is clearly seen. The Young modulus data of nonterminated graphene are within the range determined by other calculations [11] and correlate with

1 TPa proposed on the basis of experimental observations [32]. The hydrogen termination affects the data only slightly. However, we note that the region of elongation that supports the linear elastic law is rather

short in all cases, so that the graphene deformation is nonlinear and nonelastic from the very beginning. At the same time, the data related to the first stage, once the largest, scale the loading to be applied to graphene for its failure to occur.

Summarizing the obtained results, we can state the following:

the high stiffness of the graphene body is provided by the benzenoid unit;

the anisotropy of the unit mechanical behavior in combination with different configurations of unit packing with respect to the body C–C bond chains forms the ground for the structure-sensitive mechanism of mechanical behavior;

the structure sensitivity is clearly exhibited in the different response of the graphene body to either the *zg* or the *ach* deformation regime;

in contrast to on-stage deformation of the *ach* regime, the *zg* deformation mode is multistage and is particularly manifested with the formation of one-atom chains;

the difference in the behavior of *zg* and *ach* modes clearly carries the feature of these modes in the case of the benzene molecule. The observed regularities are common for both empty-edge and hydrogen-terminated nanographene. However, hydrogen termination, preserving all characteristics of empty-edge graphene in the case of the *ach* deformation mode, significantly influences the occurrence of the graphene body failure in the case of the *zg* mode, thus twice shortening the deformation area and changing the configuration of the one-atom chain.

REFERENCES

1. K. Kudin, G. E. Scuseria, and B. I. Yakobson, Phys. Rev. B **64**, 235406 (2001).

2. F. Liu, P. Ming, and J. Li, Phys. Rev. B **76**, 064120 (2007).

3. A. Hemmasizadeh, M. Mahzoon, E. Hadi, and R. Khadan, Thin Solid Films **516**, 7636 (2008).

4. X. Wei, B. Fragneaud, C. A. Marianetti, and J. W. Kysar, Phys. Rev. B **80**, 205407 (2009).

5. M. M. Shokrieh and R. Rafiee, Mater. Design **31**, 790 (2010).

6. C. Li and T.-W. Chou, Int. J. Sol. Struct. **40**, 2487 (2003).

7. A. Sakhaee-Pour, Sol. St. Comm. **149**, 91 (2009).

8. K. Hashemnia, M. Farid, and R. Vatankhah, Comput. Mat. Sci. **47**, 79 (2009).

9. J.-L. Tsai and J.-F. Tu, Mater. Design. **31**, 194 (2010).

10. Y. Guo and W. Guo, J. Phys. D **36**, 805 (2003).

11. H. Bu, Y. Chen, M. Zou, Y. Yi, and Z. Ni, Phys. Lett. A **373**, 3359 (2009).

12. G. Van Lier, C. van Alsenoy, V. van Doren, and P. Geerlings, Chem. Phys. Lett. **326**, 181 (2000).

13. Y. Gao and P. Hao, Physica E **41**, 1561 (2009).

14. M. Topsakal and S. Ciraci, Phys. Rev. B **81**, 024107 (2010).

15. C. A. Marianetti and H. G. Yevick, arXiv:1004.1849v1 [cond-mat.mtrl-sci].

16. A. Tobolski and H. Eyring, J. Chem. Phys. **11**, 125 (1943).

17. M. J. S. Dewar, Fortschr. Chem. Forsch. **23**, 1 (1971).

18. E. A. Nikitina, V. D. Khavryutchenko, E. F. Sheka, H. Barthel, and J. Weis, J. Phys. Chem. A **103**, 11355 (1999).

19. V. Khavryutchenko, E. Nikitina, A. Malkin, and E. Sheka, Phys. Low-Dim. Struct. **6**, 65 (1995).

20. V. D. Khavryutchenko and A. V. Khavryutchenko, Jr., *DYQUAMECH — Dynamical-Quantum Modelling in Mechanochemistry Software for Personal Computers*, Institute of Surface Chemistry, Nat. Ac. Sci. of Ukraine, Kiev (1993).

21. V. A. Zayets, *CLUSTER-Z1: Quantum-Chemical Software for Calculations in the s,p-Basis*, Institute of Surface Chemistry, Nat. Ac. Sci. of Ukraine, Kiev (1990).

22. E. F. Sheka and L. A. Chernozatonskii, Int. J. Quant. Chem. **110**, 1466 (2010).

23. E. F. Sheka and L. A. Chernozatonskii, Zh. Eksp. Teor. Fiz. **137**, 136 (2010).

24. P. Pulay, Theor. Chim. Acta **50**, 299 (1979).

25. E. F. Sheka, Int. J. Quant. Chem. **107**, 2803 (2007).

26. L. Kh. Sibgatullina, N. A. Popova, E. A. Nikitina, and E. F. Sheka, in *Multiscale Modeling of Nanotechnological Processes and Structures*, 2nd Allrussian Conference, Moscow (2009), p. 379.

27. N. A. Popova, L. Kh. Sibgatullina, E. F. Sheka, and E. A. Nikitina, *Mathematical Simulation in Nanotechnology*, Int. Forum on Nanotechnology 09, Moscow (2009), p. 214.

28. L. Kh. Nurullina, V. A. Popova, E. A. Nikitina, and E. F. Sheka, in *Multiscale Modeling of Nanotechnological Processes and Structures*, 2nd Allrussian Conference, Moscow (2009). p. 306.

29. E. F. Sheka, V. A. Popova, N. A. Popova, L. Kh. Nurullina, and E. A. Nikitina, *Mathematical Simulation in Nanotechnology*, Int. Forum on Nanotechnology 09, Moscow (2009), p. 341.

30. A. Chuvilin, J. C. Meyer, G. Algara-Siller, and U. Kaiser, New J. Phys. **11**, 083019 (2009).

31. C. Jin, H. Lan, L. Pen, K. Suenaga, and S. Iijima, Phys. Rev. Lett. **102**, 205501 (2009).

32. C. Lee, X. Wei, J. W. Kysar, and J. Hone, Science **321**, 385 (2008).